9-15-2022

Rapid and efficient computation of cell trajectories during ultrasonic focusing

Charles F. Babbs

Mary V. Lang

FACULTY WORKING PAPER—September 15, 2022

Rapid and efficient computation of cell trajectories during ultrasonic focusing

Charles F. Babbs and Mary V. Lang
Weldon School of Biomedical Engineering
Purdue University

ABSTRACT

This biophysical analysis explores the first-principles physics of movement of white blood cell sized particles, suspended in an aqueous fluid and experiencing progressive or standing waves of acoustic pressure. In many current applications the cells are gradually nudged or herded toward the antinodes of the standing wave, providing a degree of acoustic focusing and concentration of the cells in layers perpendicular to the direction of sound propagation. Here the underlying biomechanics of this phenomenon are analyzed specifically for the viscous regime of water--as opposed to air--and for small diameter microscopic spheroids such as living cells--as opposed to large diameter, macroscopic spheroids such as suspended polystyrene beads or levitated ping-pong balls. The resulting mathematical model leads to a single algebraic expression for the creep or drift velocity as a function of sound frequency, amplitude, wavelength, fluid viscosity, boundary dimensions, and boundary reflectivity. This expression can be integrated numerically by a very simple and fast computer algorithm to demonstrate net movement of particles as a function of time, providing a guide to optimization in a variety of emerging applications of ultrasonic cell focusing.

Key words: acoustic cytometry, acoustic levitation, acoustic microstreaming, acoustophoresis, acoustic radiation pressure, antinode, beam, cytometry, hydrodynamic focus, CD4, leukocyte, microspheres, multi-node parallel flow cytometry, particle, particle separation, particle swarm, piezoelectric, pulse-echo, radiation pressure, ultrasound, scatterer, separation, viscosity, viscous fluid

INTRODUCTION

Acoustic standing waves can move particles suspended in a fluid-filled cavity, by means of a time-averaged drift force that pushes them toward anti-nodal positions. This phenomenon is the basis for ultrasonic cell sorting[1-4]. The intuitive mechanism is that there are gradual changes in slopes of the standing pressure waves with increasing distance from each node. With every little push of the particle away from the node, it will reach a position where the restoring force pushing it back toward the node is slightly less than the original force that drove it away from the node. This process over many cycles can result in creep of the particle away from the node toward the antinode. In planar standing waves, particles typically become regularly spaced at half-wavelength intervals perpendicular to the direction of sound propagation.

The physics of acoustic radiation force acting on particles and bubbles and their subsequent motion has attracted a diverse community of thinkers over more than a century[5]. Acoustic levitation of low-density objects such as cork dust or ping-pong balls suspended in air above a loud speaker makes a fascinating demonstration[3,5-7]. A similar phenomenon is responsible for acoustic focusing of microscopic objects including cells and microspheres suspended in liquids. Several often-cited treatments of the underlying physics describe particles suspended in compressible, inviscid fluids subjected to inertial forces only in the presence of pure acoustic standing waves[8-13]. More recently, others have specifically computed analytical formulas for acoustic focusing of particles in viscous fluids such as water[14,15]; however, detailed computations are not presented. Inclusion of viscosity is important for microscopic living cells suspended in water or salt solutions, such as those in flow cytometry, especially when describing the speed of particle drift and the optimal frequencies for cell sorting[1,2].

There is an unmet need for fast, accurate computational algorithms to simulate acoustic focusing of biological cells in aqueous media. The present analysis provides a route to substantial shortening of the underlying mathematics and substantial speedup of corresponding computations by making two simplifying assumptions. The first is the explicit inclusion of fluid viscosity, while ignoring inertial forces that contribute trivially to particle creep in low Reynolds number regimes at microscopic scales. The second is computing only the net creep velocity or drift of the particle over many sound cycles, which is of interest here, rather than the fine details of oscillatory motion within each sound cycle in the time domain. These assumptions are quite reasonable for the purpose of characterizing creep or drift of biological cells in water over many thousands of sound cycles. The result is a relatively simple algebraic expression for the creep velocity of any individual cell, which can be integrated numerically over time to obtain the trajectory of the particle. For a swarm of N cells at assigned starting positions at time 0, the N trajectories can be traced over time, t , in a computer program within just one main double loop having t/dt time steps and requiring fewer than 10 lines of essential code (Table 3). The result is a rapid and efficient scheme for numerical simulation of ultrasonic cell focusing in a variety of applications and configurations. Because this approach is new, a first-principles derivation is presented.

METHODS

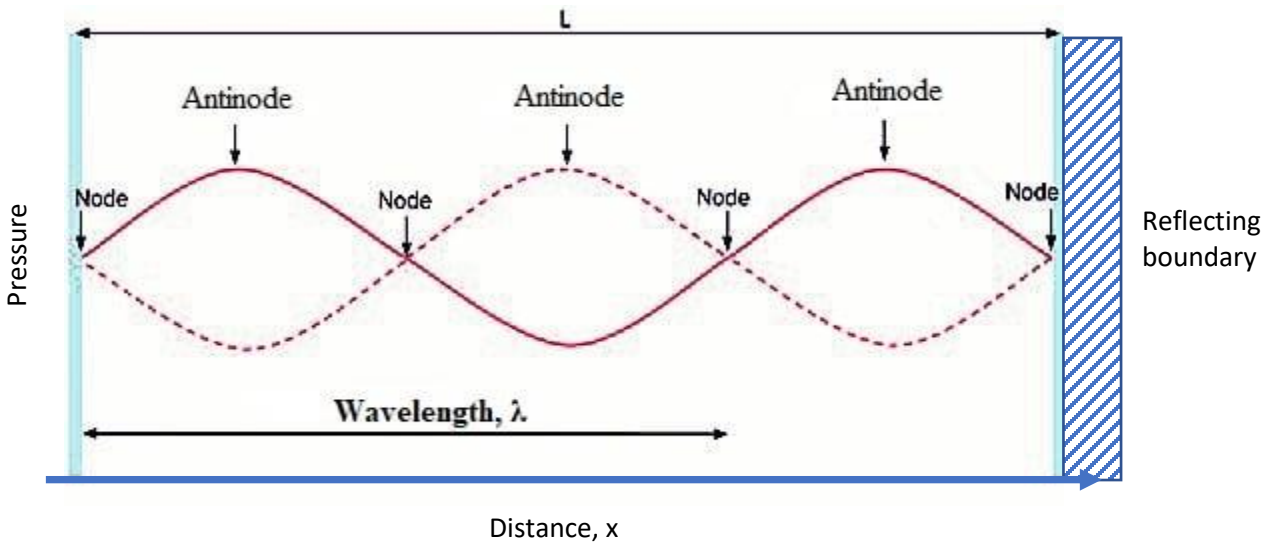

Figure 1: Model space showing the envelope of a standing wave. The pressure source is on the left, and the reflecting boundary is on the right. Solid and dashed curves show the extreme limits of the algebraic sum of incident and reflected waves. With complete reflection the combined incident and reflected waves exactly cancel at the nodes, and reinforce at the antinodes.

Figure 1 illustrates features of a standing wave created by the summation of forward and reflected plane waves. Sound waves arise on the left and are reflected at the boundary on the right. Solid and dashed curves represent the maximal excursions of the standing wave, one half cycle apart in time. At the nodes, incident and reflected waves are exactly equal amplitude and opposite in sign at all times, resulting in zero net pressure. Between nodes the combined incident and reflected waves oscillate between the solid and dashed curves.

In the present analysis we assume plane waves propagating in one dimension, x , over multiple wavelengths with negligible attenuation, as happens in water on centimeter scales. The reflected wave is inverted, and here by convention, the ratio of the peak amplitude of the reflected wave to the peak amplitude of the incident wave is a positive constant, $0 \le \phi \le 1$. A spherical particle, having radius, r , much smaller than the wavelength of sound represents a microscopic particle such as a white blood cell, located at an arbitrary distance, x , from the source. Table 1 specifies variable names for the analysis.

Table 1: Definitions

Symbol	Definition	Units (cgs)
r	Spherical particle radius	cm
A	Particle cross section, πr^2	cm^2
V_s	Spherical particle volume, $(4/3)\pi r^3$	cm^3
P(x, t)	Sinusoidal sound pressure	$dynes/cm^2$
P_{max}	Maximum positive amplitude of sound pressure	$dynes/cm^2$
b	Viscous drag coefficient	dynes/(cm/sec)
ρ	Density of surrounding fluid	g/cm^3
v	Particle velocity	cm/sec
x	Location of particle in x-dimension	cm
Δx	Change in location of particle in x-dimension	cm
v_{creep}	Particle creep (drift) velocity over many cycles	cm/sec
t	Time	sec
dt	Time step for numerical integration	sec
f	Wave frequency	Hz
$\omega = 2\pi f$	Angular wave frequency	Hz
k	Wave number	1/cm
c	Wave speed	cm/sec
η	Viscosity of surrounding fluid	g/cm/sec
ϕ	Reflection amplitude ratio	

To explore the physics of particle motion in an acoustic standing wave propagating in a viscous fluid such as water, one can begin with the classical one-dimensional equation for a sound wave without energy dissipation. The forward pressure wave is

$$P_f(x,t) = P_{max}\sin(kx - \omega t)\ , \qquad (1)$$

where P_{max} is the peak positive pressure of the wave, k is the angular wave number (k = 2π*frequency/wave speed), ω, is the angular frequency of the wave (ω = 2π*natural frequency), and t is time. The reflected wave is

$$P_r(x,t) = -\phi P_{max}\sin(kx + \omega t)\ . \qquad (2)$$

Using the identity $\sin(\alpha + \beta) = \sin(\alpha)\cos(\beta) + \cos(\alpha)\sin(\beta)$,

$$P_f(x,t) = P_{max}[\sin(kx)\cos(\omega t) - \cos(kx)\sin(\omega t)]\ , \qquad (3)$$

and

$$P_r(x,t) = -P_{max}[\phi\sin(kx)\cos(\omega t) + \phi\cos(kx)\sin(\omega t)]\ . \qquad (4)$$

The combined pressure wave, $P(x,t) = P_f(x,t) + P_r(x,t)$ is

$$P(x,t) = P_{max}[(1-\phi)\sin(kx)\cos(\omega t) - (1+\phi)\cos(kx)\sin(\omega t)] . \quad (5)$$

Now we wish to find the velocity of the particle in the sound field as a function of space and time. We assume a quasi-steady state in which the velocity of the particle in a viscous regime is always equal to its terminal velocity such that the driving force, F_P , produced by the pressure wave equals the viscous retarding or drag force on the particle, F_D . Here, for particles smaller than the wavelength of the sound pressure the driving force is directly related to the spatial gradient of the sound pressure, that is $F_P(x,t) = -\alpha\frac{\partial P(x,t)}{\partial x}$ for some positive constant, α , that depends on the size and shape of the particle. (The negative sign indicates that if pressure is lower at larger values of x , then the particle will move forward in the positive x direction.) At terminal velocity, v , the aggregate drag force (here temporarily including inertia) is $F_D(x,t) = -bv - \frac{1}{2}AC_D\rho v^2$ for viscous drag constant, b , inertial drag constant, C_D , and fluid density, ρ .

For a spherical particle, as shown in Appendix 1, the net driving force on the particle from the pressure field is $F_P(x,t) = -\frac{4}{3}\pi r^3\frac{\partial P(x,t)}{\partial x} = -V_s\frac{\partial P(x,t)}{\partial x}$ for volume, V_s of the sphere. Also, for a sphere of radius, r , viscous drag constant $b = 6\pi r\eta$ for fluid viscosity, η (Stokes' Law). A typical value of $C_D \approx 0.5$.

Continuing for a spherical particle and for $F_P = F_D$,

$$-V_s\frac{\partial P(x,t)}{\partial x} = bv + \frac{1}{2}A\rho C_D v^2 = 6\pi r\eta v + \frac{1}{2}A\rho C_D v^2 , \quad (6)$$

or

$$\frac{1}{2}A\rho C_D v^2 + 6\pi r\eta v + V_s\frac{\partial P(x,t)}{\partial x} = 0 . \quad (7)$$

One can simplify the computation for ultrasonic focusing of biological cells by noting that viscous forces dominate.

In viscous regimes we have $\left(\frac{1}{2}C_D\rho v^2\right)/(6\pi r\eta v) \approx 0$ and

$$v \approx \frac{-V_s}{6\pi r\eta}\frac{\partial P(x,t)}{\partial x} = \frac{-V_s}{b}\frac{\partial P(x,t)}{\partial x} \quad (8)$$

for drag constant, b .

To determine if this simplification is justified, one may estimate the ratio of inertial to viscous forces (Reynolds number), namely

$$\frac{F_{inert}}{F_{visc}} = \frac{\frac{1}{2}A\rho C_D v^2}{6\pi r\eta v} . \quad (11)$$

For spherical particles with $C_D \approx \frac{1}{2}$, one would have an inertial to viscous ratio of about

$$\frac{F_{inert}}{F_{visc}} = \frac{1}{4}\frac{\pi r^2 \rho v}{6\pi r \eta} = \frac{1}{24}\frac{r\rho v}{\eta} . \quad (12)$$

If this ratio is << 1, then the system is viscous. If the ratio is >> 1 then the system is inertial.

For the case of a 10-micron radius cell in water, moving at a speed of 1 cm/sec, the ratio is

$$\frac{F_{inert}}{F_{visc}} = \frac{1}{24}\frac{0.001\ \text{cm} \cdot 1\frac{g}{cm^3} \cdot 1\frac{cm}{sec}}{0.01\frac{g}{cm \cdot sec}} = \frac{1}{240} \ll 1 . \quad (13)$$

Hence, for simplicity we can consider viscous forces to be dominant in the cell focusing problem, so that Equation (8) applies.

Differentiating Equation (5) with respect to x ,

$$\frac{\partial P(x,t)}{\partial x} = P_{max} k[(1-\phi)\cos(kx)\cos(\omega t) + (1+\phi)\sin(kx)\sin(\omega t)] , \quad (14)$$

so that

$$v \approx \frac{-V_s}{b} P_{max} k[(1-\phi)\cos(kx)\cos(\omega t) + (1+\phi)\sin(kx)\sin(\omega t)] . \quad (15)$$

Particle creep and speedup of numerical computations

Equation (15) implies that in the time domain particle velocity is a sinusoidal function at angular frequency, ω, as can also be appreciated intuitively from Figure 1. As time proceeds, the particle is rapidly oscillating between forward and backward directions in the x-domain. However, because of the curvature of the force field in the x-domain, the average force on the particle during forward movement during one half cycle time will be slightly different than the average force on the particle during the previous half cycle time. This subtle nonlinear effect will result in creep of the particle in x-dimension over many cycles. It is this gradual net movement of the particle over many time cycles that is of particular interest here.

Equation (15) can be solved for velocity, v , numerically over many small time steps, dt , starting with initial values of x and integrating velocity, v , over time to obtain updated values of x , etc. For ultrasonic frequencies this approach requires very small time steps numbering > 100 per cycle, and long computation times.

To focus specifically on particle creep, and also to speed numerical integration in the time domain, consider the time average pressure gradient of the particle over two half cycles of sound pressure, the first half cycle from ωt = 0 to π radians and the second half cycle from ωt = π to 2π radians. During the first half cycle the mean value of pressure gradient will be

$$\left(\frac{\partial P}{\partial x}\right)_1 = P_{max} k \left[\frac{2}{\pi}(1+\phi)\cos(kx)\right], \quad (16)$$

where the mean value of the sine function from ωt = 0 to ωt = π radians is 2/π and mean value of the cosine function from ωt = 0 to ωt = π radians is 0. Similarly, from π to 2π radians the mean value of the sine function is –2/π and mean value of the cosine function is 0, so that during the second half of the sound cycle

$$\left(\frac{\partial P}{\partial x}\right)_2 = P_{max} k \left[-\frac{2}{\pi}(1+\phi)\cos(k(x+\Delta x_1))\right], \quad (17)$$

where Δx_1 is the corresponding change in position, x , of the particle over the first half cycle.

Here we assume that $\Delta x_1 \ll \lambda$ for wavelength, $\lambda = c/f$, and also $\Delta x_1 \ll x$. Then, using the identity $\cos(\alpha+\beta) = \cos(\alpha)\cos(\beta) - \sin(\alpha)\sin(\beta)$, in which for small β << 1, cos(β) ≈ 1 and sin(β) ≈ β , we have

$$\left(\frac{\partial P}{\partial x}\right)_2 \approx P_{max} k \left[-\frac{2}{\pi}(1+\phi)\left(\cos(kx) - \sin(kx)\, k\Delta x_1\right)\right]. \quad (18)$$

Combining Equations (16) and (18) , the time averaged gradient over one full cycle is

$$\overline{\left(\frac{\partial P}{\partial x}\right)} \approx \frac{P_{max}}{\pi} k(1+\phi)\sin(kx)\, k\Delta x_1 . \quad (19)$$

Using Equation (16) and the duration of the first half period as 1/(2f) for natural frequency, f ,

$$\Delta x_1 = \frac{v}{2f} = \frac{V_s}{2bf} P_{max} k \left[\frac{2}{\pi}(1+\phi)\cos(kx)\right] = P_{max}\frac{V_s k}{\pi b f}(1+\phi)\cos(kx), \quad (20)$$

in correct units of $\frac{dyn}{cm^2} \cdot \frac{cm^2}{\frac{dyn-sec}{cm}\frac{1}{sec}} = cm$, where the units of viscous drag constant, b = 6πrη , are dynes / (cm/sec).

Combining Equations (19) and (20),

$$\overline{\left(\frac{\partial P}{\partial x}\right)} \approx \frac{P_{max}}{\pi} k(1+\phi)\sin(kx)\, k\left(P_{max}\frac{V_s k}{\pi b f}(1+\phi)\cos(kx)\right), \quad (21)$$

and collecting terms

$$\overline{\left(\frac{\partial P}{\partial x}\right)} \approx \left(\frac{P_{max}}{\pi} k(1+\phi)\right)^2 \frac{V_s k}{bf}\sin(kx)\cos(kx) \quad (22)$$

in units of $\left(\frac{dyn}{cm^2}\frac{1}{cm}\right)^2 \cdot \frac{cm^2}{\frac{dyn-sec}{cm}\frac{1}{sec}} = \left(\frac{dyn}{cm^2}\right)\frac{1}{cm} cm$, as expected.

So, the combined positive and negative creep over one full cycle in the viscous regime is

$$\Delta x_1 + \Delta x_2 = \frac{\bar{v}}{f} = \frac{V_s}{bf}\left(\overline{\frac{\partial P(x,t)}{\partial x}}\right) \approx \frac{V_s}{bf}\left(\frac{P_{max}}{\pi} k(1+\phi)\right)^2 \frac{V_s k}{bf} \sin(kx)\cos(kx) \quad (23)$$

or

$$\Delta x_1 + \Delta x_2 \approx \left(\frac{P_{max}}{\pi} k \frac{V_s}{bf}(1+\phi)\right)^2 k \sin(kx)\cos(kx) \quad (24)$$

in correct units of $\left(\frac{dyn}{cm^2}\frac{cm^2 \cdot sec}{\frac{dyn-sec}{cm}}\right)^2 \frac{1}{cm} = cm$.

Further, applying the identity $\sin(\alpha)\cos(\alpha) = \frac{1}{2}\sin(2\alpha)$,

$$\Delta x_1 + \Delta x_2 \approx \frac{1}{2}\left(\frac{P_{max}}{\pi} k \frac{V_s}{bf}(1+\phi)\right)^2 k \sin(2kx) . \quad (25)$$

This is a compact expression for the creep of the particle with each full cycle of pressure under dominant viscous conditions.

The rate of creep per second, or creep velocity, v_{creep} , equals $\Delta x_1 + \Delta x_2$, which is a function of $(1/f)^2$, divided by cycle time, $1/f$, namely

$$v_{creep} \cong \frac{1}{2f}\left(\frac{P_{max}}{\pi}\frac{V_s}{b}(1+\phi)\right)^2 k^3 \sin(2kx) . \quad (26)$$

Substituting for angular wave number, $k = 2\pi/\lambda$, for wavelength, λ ,

$$v_{creep} \cong \frac{1}{2f}\left(\frac{P_{max}}{\pi}\frac{V_s}{b}(1+\phi)\right)^2 \frac{8\pi^3}{\lambda^3}\sin(4\pi x/\lambda) \text{ , or} \quad (27)$$

$$v_{creep} \cong \frac{4\pi}{f\lambda}\left(P_{max}\frac{V_s}{b\lambda}(1+\phi)\right)^2 \sin(4\pi x/\lambda) \quad (28)$$

in units of $\frac{sec}{cm}\left(\frac{cm}{sec}\right)^2 = \frac{cm}{sec}$.

Now consider a spherical particle with radius, r , cross section πr^2. In this case the Stokes' Law coefficient of friction is $b = 6\pi r\eta$ for fluid viscosity, η .

$$v_{creep} \cong \frac{4\pi}{f\lambda}\left(P_{max}\frac{V_s}{6\pi r\eta\lambda}(1+\phi)\right)^2 \sin(4\pi x/\lambda) , \quad (29)$$

and substituting $\frac{4}{3}\pi r^3$ for the volume, V_s , of the sphere,

$$v_{creep} \cong \frac{4\pi}{f\lambda}\left(P_{max}\frac{4}{3}\cdot\frac{r^2}{6\eta\lambda}(1+\phi)\right)^2 \sin(4\pi x/\lambda)\,. \quad (30)$$

Noting that the fraction $4^3/(18^2) = 0.1975 \approx 1/5$,

$$v_{creep} \approx \frac{1}{5}\frac{\pi}{f\lambda}\left(P_{max}\frac{r^2}{\eta\lambda}(1+\phi)\right)^2 \sin(4\pi x/\lambda)\,. \quad (31)$$

This is a compact expression for creep velocity as a function of position, x. It is sinusoidal, changing from positive to negative values as a function of x only. At locations $4\pi x/\lambda = n\pi$ for n = 1, 2, 3, … or $x/\lambda = 1/4\,, 2/4\,, 3/4$, and so on, $v_{creep} \approx 0$. These points are the nodes and antinodes of the standing wave. For $0 < x/\lambda < ¼$, v_{creep} is positive. Throughout this range of x , particles will creep forward in the x-direction toward position $x/\lambda = ¼$. For $¼ < x/\lambda < ½$, v_{creep} is negative. Throughout this range of x , particles will creep backward in the x-direction toward position $x/\lambda = ¼$. Thus, in the range For $0 < x/\lambda < ½$, the particles will tend to clump together one quarter wavelength from the origin. Similarly, particles will tend to clump together at two quarters of one wavelength from the origin, and so on. These points of concentration are the antinodes of the standing wave (Figure 1).

The nodes exhibit unstable equilibria (see Figure 1) such that only particles at the exact peaks of the standing waves will have zero creep. Perturbations in their x-location will lead to a slippery slope. The antinodes, however, exhibit stable equilibria. Despite perturbations, once a particle migrates to an antinode, it will creep no more; instead, it will undergo small symmetrical oscillations at the sonic frequency. Equation (31) predicts that nearly all particles will creep toward the nearest antinode and clump together there.

Interesting rearrangements of Equation (31) are possible. Noting that frequency x wavelength = sound speed, $f\lambda = c$, Equation (31) can be written as

$$\frac{v_{creep}}{c} \approx \frac{1}{5}\pi\left(\left(\frac{P_{max}}{f\eta}\right)\left(\frac{r}{\lambda}\right)^2(1+\phi)\right)^2 \sin\left(4\pi\left(\frac{x}{\lambda}\right)\right) \quad (32)$$

in terms of dimensionless creep velocity, $\frac{v_{creep}}{c}$, dimensionless pressure, $\left(\frac{P_{max}}{f\eta}\right)$, and dimensionless radius, $\left(\frac{r}{\lambda}\right)$. In this form, it is evident that the creep velocity depends strongly on the ratio of pressure to frequency and very strongly on the ratio of particle size to wavelength. Creep is four times faster for complete standing waves with $\phi = 1$ than for waves without reflection ($\phi = 0$). However, even without reflection, particles will creep, as happens in acoustic levitation by single beam trapping[6].

To speed numerical computation of particle motion, one can realize that $\Delta x_1 + \Delta x_2$ on each sound cycle is quite small compared to position, x , so that v_{creep} is stable over tens of cycles. Hence, one can use classical numerical techniques, such as the simple Euler method, to integrate creep velocity over time in order to determine the total displacement of a particle from any chosen starting position, x . The time step for numerical integration of creep velocity can be longer than the period of the sound wave, namely 1/f . In this way one can quickly calculate movements of a population of particles in space and time for any chosen set of model parameters.

NUMERICAL METHODS AND RESULTS

To explore the feasibility of ultrasonic clumping or herding of white blood cells in spinal fluid, Equation (31) was solved for a set of particles specified in Table 2.

Table 2: Standard model parameters

Symbol	Definition	Value	Units (cgs)
r	Spherical particle radius	0.00075	cm
P_{max}	Maximum positive amplitude of sinusoidal sound pressure	200000	dynes/cm^2
f	Wave frequency	500000	Hz
c	Wave speed	148000	cm/sec
η	Fluid viscosity (that of water)	0.01	g/cm/sec
ϕ	Reflection amplitude ratio	0--1	
dt	Time step for integration	0.0002	sec

To track the behavior of a much larger population, NCELLS = 200 spherical particles, representing a statistical sample of white blood cells in isotonic saline solution, were positioned randomly at time zero in a space 1 cm deep, ranging from x = 0 to x = 1.0 cm. The plane wave ultrasonic source was located at x = 0. The creep of each particle, n , in the vertical, x-direction was calculated by numerically integrating creep velocity from Equation (31) as function of time using the simple Euler method (cellx(n) = cellx(n) + vcreep * dt) with time step dt = 0.0002 sec. Table 3 illustrates the computational algorithm in the form of pseudocode, showing the essential logical steps, with self-evident variable names and lumped Print() functions that output positions of all of the cells after every “SkipNumber” of time steps, dt .

Table 3: Abbreviated algorithm for computation of particle creep

```
ntimepoints = SimulationTime/dt

For i = 0 To ntimepoints

   For n = 1 To NCELLS

      "get creep velocity"
      vcreep = (0.2 * PI / WAVESPEED) * _
      (Pmax * CELLradius ^ 2 / VISCOSITY / lambda) ^ 2 _
      * (1 + REFLECTIONCOEFF) ^ 2 * Sin(4 * PI * cellx(n) / lambda)

      "update cell position"
      cellx(n) = cellx(n) + vcreep * dt

      "implement boundary conditions"
      If cellx(n) < 0 Then cellx(n) = 0
      If cellx(n) > xmax Then cellx(n) = xmax

   Next n

   If i Mod SkipNumber = 0 Then
      "update cell position table for chart"
      For n = 1 To NCELLS
         PrintTime()
         PrintCellPositions()
      Next n
  End If

Next i
```

Figure 2 shows distributions of typical cell populations in the 1 x 1 cm^2 model space at 0, 2, 4, and 8 seconds after the onset of sound pressure. The initial random distributions of cells for each simulation were separately determined in each case. The reflection coefficient, representing the boundary at x = 1.0 cm, was $\phi = 0.5$. The wavelength of the ultrasound was $\lambda = 0.30$ cm. Particles become concentrated in bands about 0.15 cm or one-half wavelength apart. These are the antinodes. Note that it only takes ~ 100 tracer particles to represent a much larger particle swarm.

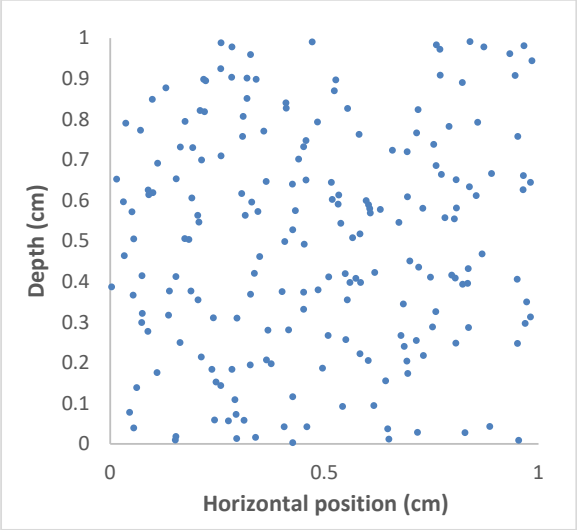

0 sec

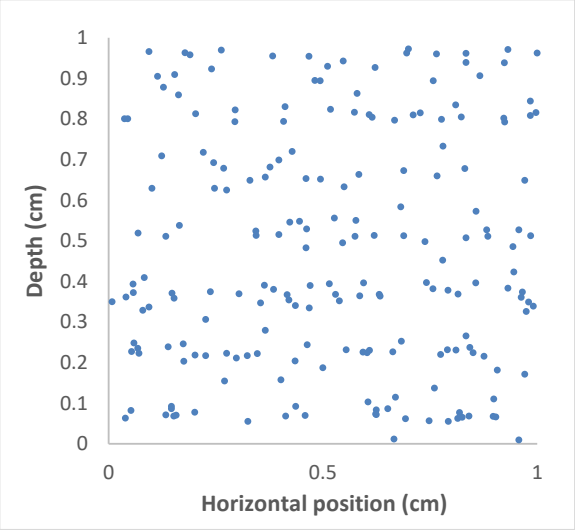

2 sec

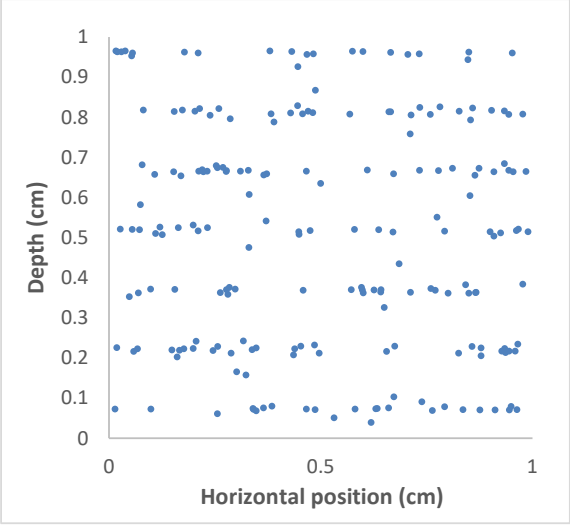

4 sec

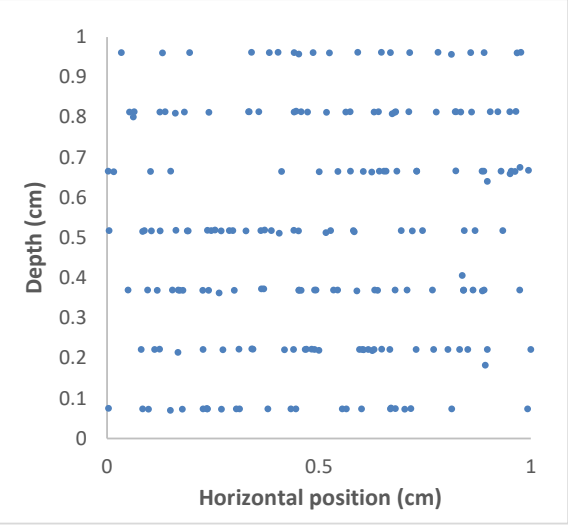

8 sec

Figure 2: 1 x 1 cm model space filled with a sample of simulated white blood cells in isotonic saline solution and subjected to plane wave ultrasound from a source at zero depth. The reflection coefficient, representing the boundary at x = 1.0 cm, was $\phi = 0.5$. Wavelength $\lambda = 0.30$ cm.

Figure 3 shows a set of simulations lasting 3 seconds for different values of the reflection coefficient, ϕ. Banding occurs to a lesser degree with reduced reflection coefficient but is still present with zero reflection.

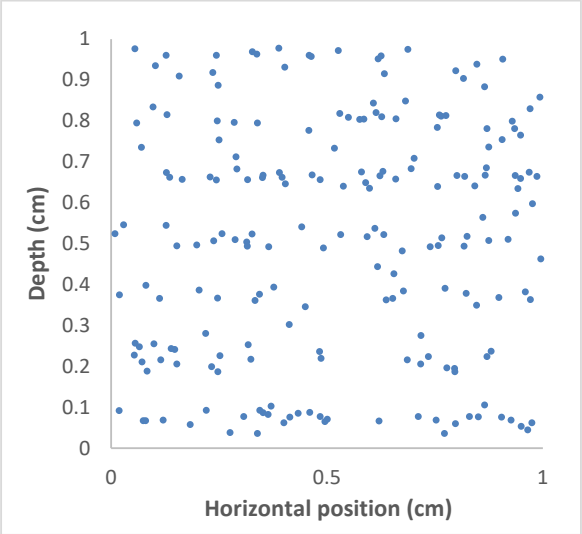

ϕ = 0.00

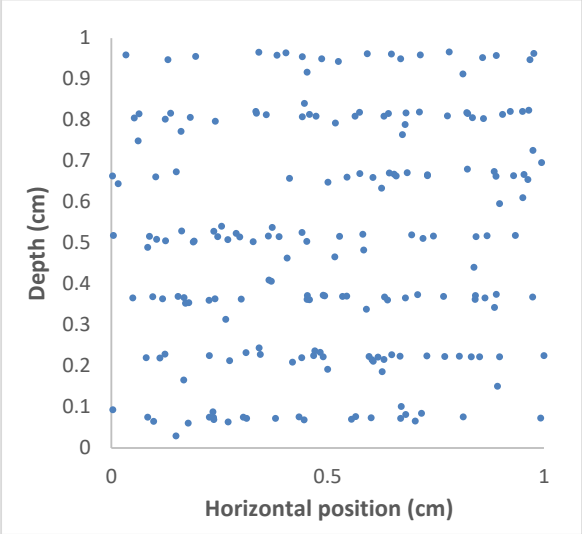

ϕ = 0.33

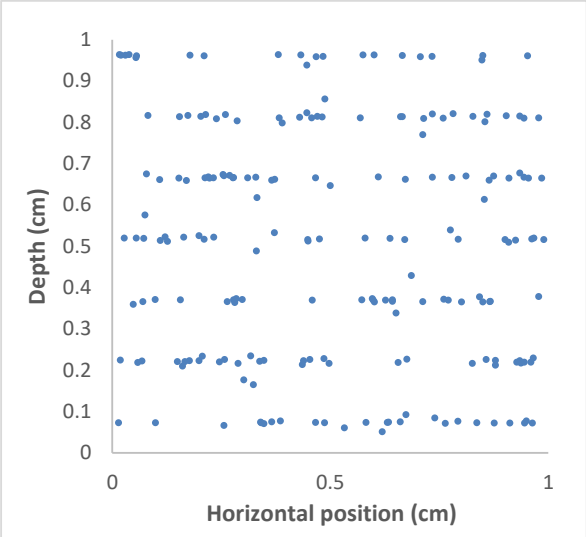

ϕ = 0.67

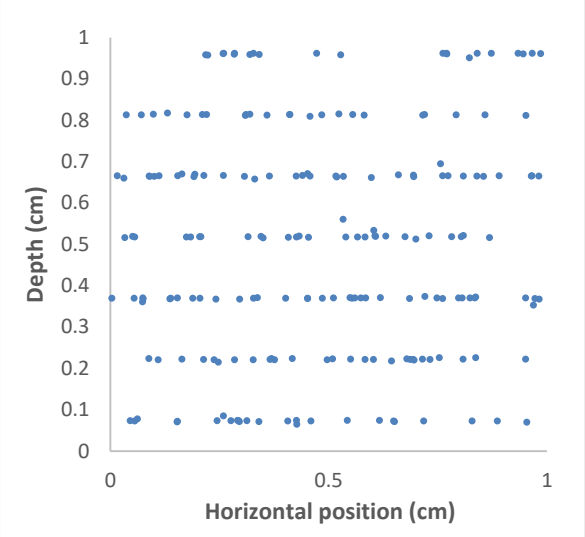

ϕ = 1.00

Figure 3: 1 x 1 cm model space filled with a sample of simulated white blood cells in isotonic saline solution and subjected to plane wave ultrasound from a source at zero depth. The reflection coefficient, representing the boundary at x = 1.0 cm, ranges from ϕ = 0.0 to 1.0. Wavelength λ = 0.30 cm. Total simulation time was 3.0 seconds.

Re-arranging Equation (31) a different way and using $f\lambda = c$,

$$v_{creep} \approx \frac{1}{5}\frac{\pi}{c}\left((P_{max}f)\frac{r^2}{\eta c}(1+\phi)\right)^2 \sin(4\pi x f/c)\ . \qquad (33)$$

This expression implies that a constant creep velocity will happen if the product of pressure and frequency is constant; however, the antinodes will occur closer together as frequency is increased. Figure 4 shows snapshots for this scenario after 4 seconds. This phenomenon suggests that there is a critical range of frequencies for cell clumping and concentration using ultrasound. At frequencies that are too high, the cells still appear quasi-randomly scattered in closely spaced bands, such as in (A), containing fewer cells in each band. At more ideal frequencies, such as in (B), there are a few prominent bands. At frequencies that are too low, the bands of cells may be too far apart and aggregate out of the field of view of ultrasonic imaging.

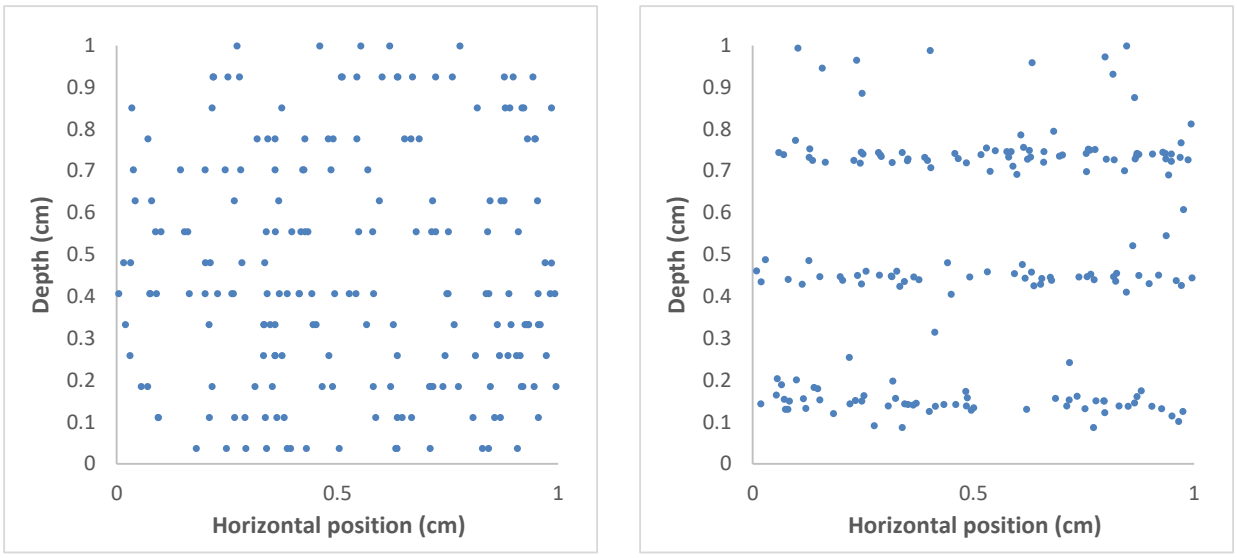

(A) (B)

Figure 4: 1 x 1 cm model space filled with a sample of simulated white blood cells in isotonic saline solution and subjected to plane wave ultrasound from a source at zero depth. The reflection coefficient, representing the boundary at x = 1.0 cm, is 1.0. (A) half standard frequency and twice standard P_{max}, compared to Table 1 parameters. (B) twice standard frequency and half standard, P_{max} , compared to Table 1 parameters.

Focusing on viscous forces and ignoring trivial inertial forces enhances both the accuracy and speed of the computational approach described here. Originally conceived as a phenomenon occurring in stationary standing waves only, such clumping behavior is here shown to occur also in partial standing waves created by incomplete reflection.

DISCUSSION

Acoustic focusing of cells is an emerging and exciting technology with a bright future[1,2,16,17]. One major application being studied currently is in the field of flow cytometry. Piyasena and coworkers in New Mexico[1], developed and tested multi-node acoustic focusing flow cells that can position 10 to 100 micron diameter particles into as many as 37 parallel flow streams. The authors could precisely position human white blood cells for a CD4+ cell analysis. Potential applications for creating multiple parallel channels include detection of rare circulating tumor cells in peripheral blood samples and detection of fetal cells in maternal blood for prenatal diagnosis.

Another interesting application of acoustic focusing is the manipulation of living microorganisms[18], such as euglena and paramecia using ~3 MHz ultrasonic standing waves. Such ultrasonic focusing of bacteria may be applicable for in vivo clinical testing in patients. A potential example is provided by the work of Stevenson et al.[19] demonstrating streaks or layers of bladder "debris" on ultrasound as a predictor for positive urine cultures in a pediatric population. Similar findings were reported in adults by Wachsberg and coworkers[20]. These ultrasonically visualized debris layers (likely containing both bacteria and white blood cells) perpendicular to the ultrasonic beam--even in mild cases (Fig 1A in [19])--look remarkably like the patterns of particle clumping seen in other experimental systems, including, colored zeolite particles[12], human leukemia cells[21], antibody coated microspheres[4], and 10 micron diameter, 1.05 g/ml density polystyrene microspheres[22], as well as in the simulations show in in Figures 2 through 4 above.

Another intriguing possibility that emerges from the present study is related to the rapid, painless, and noninvasive diagnosis of bacterial meningitis, especially in small children. Scattered white blood cells suspended in cerebrospinal fluid could be induced to clump together percutaneously using a hand-held device to make a bigger target that is much easier to detect with ultrasound than individual cells, thus making it possible to test for bacterial meningitis quickly, painlessly, and noninvasively.

CONCLUSIONS

In all of these avenues of applied science and product development, rapid and efficient simulation of cell focusing on an ordinary laptop computer may provide a helpful tool to explore potential optimal solutions in a multi-dimensional feature space including particle size, frequency, reflectivity of boundaries, time, and other factors at little marginal cost.

APPENDIX: net force on sphere in an x-directed pressure gradient

Figure A1 shows a sketch of a spherical particle suspended in a fluid pressure gradient along the x-dimension. The radius of the particle is denoted r. The x coordinate of the center of the sphere is denoted 0 .

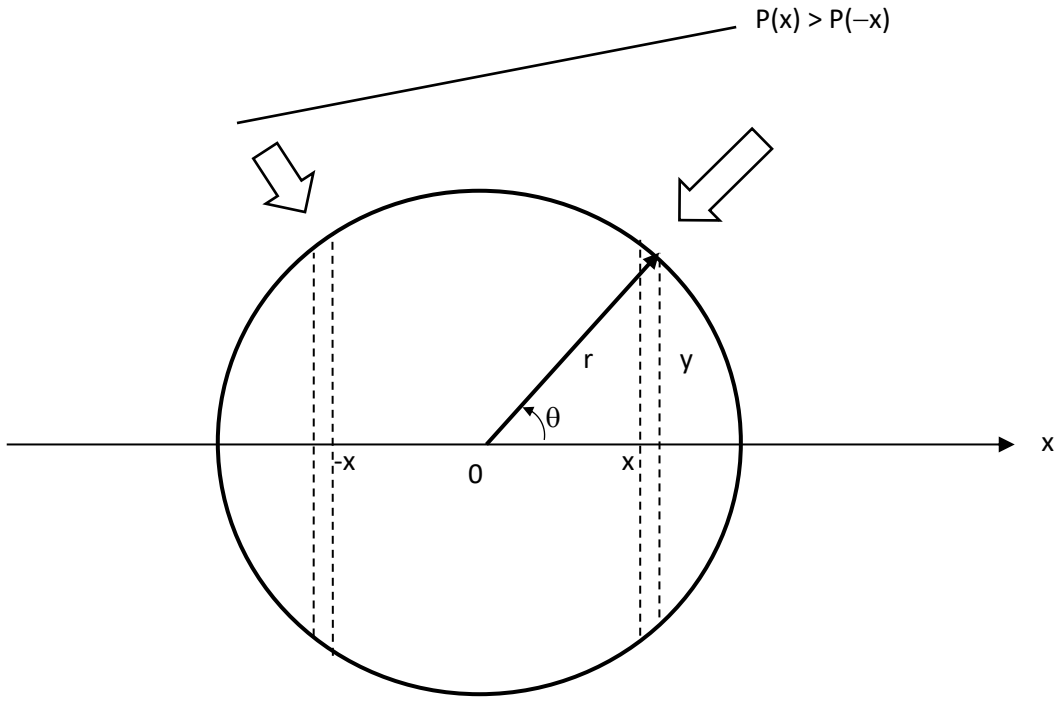

Figure A1: Idealized spherical particle in a pressure gradient along the x-dimension. Particle radius is r. Pressure pushes perpendicular to the surface of the sphere at all levels.

Variable orthogonal distances from the center of the particle are denoted x and y, as shown, where $x = r\cos\theta$ and $y = r\sin\theta$. The pressure varies as a plane wave along the x-dimension according to wave function P(x, t). Like ocean pressure at depth, the pressure exerts force perpendicular to the surface of the sphere at all points on the surface. Consider two differential ring-like slices of the surface at –x and +x , perpendicular to the x-y plane. The circumferential surface area of each slice is

$dS = 2\pi y r d\theta = 2\pi r^2 \sin\theta d\theta$.

For each pair of differential slices the positive, x-directed forces on the sphere are $dF_x^+ = dS \cdot P(-x,t)\cos\theta$, pushing to the right, and $dF_x^- = dS \cdot P(x,t)\cos\theta$, pushing to the left. The net force,

$$dF_x = dF_x^+ + dF_x^- = -dS \cdot \cos\theta[P(x,t) - P(-x,t)]$$

or

$$dF_x = -2\pi r^2 \sin\theta d\theta \cdot \cos\theta[P(x,t) - P(-x,t)] .$$

Since radius r is much less than the pressure wavelength, the local pressure slope is essentially constant, and equal to the pressure slope at the center of the sphere, $\left(\frac{\partial P}{\partial x}\right)_0$. In turn,

$$dF_x = -2\pi r^2 \sin\theta d\theta \cos\theta \left[\left(\frac{\partial P}{\partial x}\right)_0 2r\cos\theta\right] = -4\pi r^3 \left(\frac{\partial P}{\partial x}\right)_0 \sin\theta\cos^2\theta d\theta .$$

The total net force on the sphere is

$$F_x = -4\pi r^3 \left(\frac{\partial P}{\partial x}\right)_0 \int_0^{\pi/2} \sin\theta\cos^2\theta d\theta .$$

Consulting a table of integrals, $\int \sin\theta\cos^2\theta d\theta = -\frac{\cos^3}{3}$, so that

$$F_x = -\frac{4}{3}\pi r^3 \left(\frac{\partial P}{\partial x}\right)_0 .$$

If $\left(\frac{\partial P}{\partial x}\right)_0 > 0$ then $F_x < 0$ and vis versa. For the volume of a sphere $V_s = \frac{4}{3}\pi r^3$

$$F_x = -V_s \left(\frac{\partial P}{\partial x}\right)_0 .$$

REFERENCES

1. Piyasena ME, Austin Suthanthiraraj PP, Applegate RW, Jr., Goumas AM, Woods TA, et al. (2012) Multinode acoustic focusing for parallel flow cytometry. Anal Chem 84: 1831-1839.
2. Laurell T, Petersson F, Nilsson A (2007) Chip integrated strategies for acoustic separation and manipulation of cells and particles. Chem Soc Rev 36: 492-506.
3. Marzo A, Drinkwater BW (2019) Holographic acoustic tweezers. Proc Natl Acad Sci USA 116: 84-89.
4. Wiklund M, Toivonen J, Tirri M, Hanninen P, Hertz HM (2004) Ultrasonic enrichment of microspheres for ultrasensitive biomedical analysis in confocal laser-scanning fluorescence detection. Journal of Applied Physics 96: 1242-1248.
5. Sarvazyan AP, Rudenko OV, Nyborg WL (2010) Biomedical applications of radiation force of ultrasound: historical roots and physical basis. Ultrasound Med Biol 36: 1379-1394.
6. Andrade MAB, Marzo AB, Adamowski JC (2020) Acoustic levitation in mid-air: Recent advances, challenges, and future perspectives. Applied Physics Letters 116: 250501.

7. Perez N, Andrade NAB, Canetti R, Adamowski JC (2014) Experimental determination of the dynamics of an acoustically levitated sphere. Journal of Applied Physics 116: 184901-184908.
8. Gorkov LP (1962) On the forces acting on a small particle in an acoustical field in an ideal fluid. Soviet Physics, Doklady 6: 773-775.
9. King LV (1934) Proc Roy Soc A147: 212-240.
10. Nyborg WL (1967) Radiation Pressure on a Small Rigid Sphere. Journal of the Acoustical Society of America 42: 947-952.
11. Wu JR, Du GH, Work SS, Warshaw DM (1990) Acoustic radiation pressure on a rigid cylinder: an analytical theory and experiments. J Acoust Soc Am 87: 581-586.
12. Ostasevicius V, Jurenas V, Golinka L, Gaidys R, Aleksa A (2018) Separation of Microparticles from Suspension Utilizing Ultrasonic StandingWaves in a Piezoelectric Cylinder Actuator. Actuators 7: 1-12.
13. Cosgrove JA, Buick JM, Campbell DM, Greated CA (2004) Numerical simulation of particle motion in an ultrasound field using the lattice Boltzmann model. Ultrasonics 43: 21-25.
14. Settnes M, Bruus H (2012) Forces acting on a small particle in an acoustical field in a viscous fluid. Phys Rev E Stat Nonlin Soft Matter Phys 85: 016327.
15. Doinikov A (1994) Acoustic radiation pressure on a compressible sphere in a viscous fluid. Journal of Fluid Mechanics 267: 1-22.
16. Ward MD, Kaduchak G (2018) Fundamentals of Acoustic Cytometry. Curr Protoc Cytom 84: e36.
17. Wiklund M, Hertz HM (2006) Ultrasonic enhancement of bead-based bioaffinity assays. Lab Chip 6: 1279-1292.
18. Saito M, Kitamura N, Terauchi M (2002) Ultrasonic manipulation of locomotive microorganisms and evaluation of their activity Journal of Applied Physics 92: 7581.
19. Stevenson SM, Lau GA, Andolsek WC, Presson AP, Cartwright PC (2018) Bladder debris on ultrasound as a predictor for positive urine culture in a pediatric population. J Pediatr Urol 14: 254 e251-254 e255.
20. Wachsberg RH, Festa S, Samaan P, H.J. E, Baker SR (1998) Particulate Echoes within the Bladder Detected with Transvaginal Sonography: A Sign of Urinary Tract Infection? Emergency Radiology May/June: 137-139.
21. Lee YH, Peng CA (2007) Nonviral transfection of suspension cells in ultrasound standing wave fields. Ultrasound Med Biol 33: 734-742.
22. Woodside SM, Bowen BD, Piret JM (1997) Measurement of Ultrasonic Forces for Particle-Liquid Separations. AIChE Journal 43: 1727-1736.